J. Synchrotron Rad. (1999). **6**, 979–984

A focusing multilayer analyser for local diffraction studies

U. Lienert,[a,b]* H. F. Poulsen,[b] V. Honkimäki,[a] C. Schulze[c] and O. Hignette[a]

[a]ESRF, F-38043 Grenoble CEDEX, France, [b]Materials Research Department, Risø National Laboratory, DK-4000 Roskilde, Denmark, and [c]Swiss Light Source, PSI, CH-5232 Villigen PSI, Switzerland. E-mail: lienert@esrf.fr

(*Received 10 August 1998; accepted 29 January 1999*)

A novel X-ray diffraction technique for the local structural characterization of thick specimens is presented. Broad energy-band focusing elements are used both on the incoming and exit (diffracted) side of the sample. The geometry allows imaging, and magnification, of a line through the thickness of the sample. In comparison with conventional methods of defining three-dimensional gauge volumes the new technique provides superior depth resolution, higher flux, and a remedy for some systematic errors occurring in strain measurements due to, for example, grain size effects. The technique is validated by a synchrotron test experiment using a bent and meridionally graded multilayer as the focusing analyser element. The incoming beam is monochromated, at 30 keV, and focused to a 15 µm spot size by means of a bent Laue crystal. The resulting depth profile from the (222) reflection of a 21 µm-thick rolled Au foil has a width of 44 µm. The depth resolution, magnification and reflectivity as a function of the energy bandwidth are found to be well matched by theory. The prospect of the technique and the associated aberrations are discussed.

Keywords: X-ray optics; lattice strains.

1. Introduction

Three-dimensional structural characterization of thick samples is of considerable interest in metallurgy and related scientific fields, where surface investigations often do not represent bulk behaviour. Measured materials properties can be strain or the orientation, size or shape of grains. As such, neutron diffraction techniques with spatial resolutions of approximately $1 \times 1 \times 1$ mm^3 are widely used to map out stress and strain fields (*e.g.* Allen *et al.*, 1985).

Recently, it has been shown that the spatial resolution can be vastly improved by using high-energy X-ray diffraction ($E > 40$ keV) from third-generation synchrotron sources (Poulsen *et al.*, 1997). X-rays in this energy range have penetration depths of millimetres in typical metals. Moreover, efficient optical devices based on bent Laue crystals and/or multilayers have been demonstrated that can focus and monochromatize the beam from such sources (Lienert *et al.*, 1998). The flux in the focal spot is thereby increased by up to six orders of magnitude as compared with a conventional set-up with a flat perfect crystal monochromator. It should be remembered that broad-band optics do not prevent strain measurements, as the position of the centres of diffraction peaks can typically be determined to within 1% of their width.

In order to take full advantage of these developments it is necessary to reconsider the way depth information is obtained. Conventionally, this is performed by cross-beam techniques, where both the incoming and the exit (diffracted) beams are confined by collimators. For the case of high-energy X-rays such an approach poses two major problems, discussed below.

Firstly, in order to absorb the hard X-rays efficiently, collimators have to be of the order of millimetres in length. At the same time, in order to maintain depth resolution, collimator gaps have to be smaller at higher energies due to the smaller Bragg angles. Moreover, the collimators will often need to be placed at some distance from the sample due to restrictions made by the sample environment, *e.g.* furnaces or stress rigs, which again tend to deteriorate the depth resolution. In total these effects imply that collimator openings must have large aspect ratios of 10^3–10^4. Hence, manufacturing becomes complicated and the exit collimator will have a narrow angular acceptance. This in turn prohibits an efficient focusing scheme for the incoming beam, thereby diminishing the available flux.

Secondly, it is well known that the use of a collimator on the exit side can give rise to systematic errors in strain determinations, when sample characteristics are inhomogeneous on the scale of the resolution (Webster *et al.*, 1996; Lorentzen, 1997), *e.g.* due to grain size effects.

Here we propose an alternative approach for defining the local volume, where broad-band focusing optics are used on the exit as well as the incoming side. We will use the term ‘focusing analysing optics’ for this principle. On the exit side a bent and meridionally graded multilayer is used to image a line along the monochromatic beam in the sample onto a line perpendicular to the exit beam direction. It is shown theoretically as well as experimentally that such

© 1999 International Union of Crystallography
Printed in Great Britain – all rights reserved

ISSN 0909-0495 © 1999

a set-up gives superior depth resolution without any of the problems associated with the use of collimators. We start by introducing the geometry and basic concepts of the focusing analysing optics. Next, results of a synchrotron test experiment are presented and compared with model calculations for aberration-free optics. Finally, we discuss the prospect of the technique. The work is restricted to focusing in one plane only.

2. Optics principle

A general analysis of the imaging properties of the focusing analysing optics is beyond the scope of this paper. Instead we elucidate the principal ideas of the particular experimental setting used in the synchrotron test experiment.

A sketch of the set-up is shown in Fig. 1. Focusing of the incoming beam is obtained by means of a bent Laue monochromator. The focused beam has an energy gradient $\Delta E/E$ of the order of 1%. A periodic multilayer is bent into an elliptical shape and positioned behind the sample such that a point B in the sample coincides with one of the focal points. For a given reflection, all rays from B will be focused onto the other focal point B^*. All rays from other points in the sample such as A will similarly be imaged onto (broadened) spots such as A^*. We define the object plane as the plane that contains the focal point B and is perpendicular to the beam that impinges onto the multilayer. The image plane contains the focal point B^* and is perpendicular to the diffracted beam. Let h_p be the projection of the vector **AB**, of length s, onto the object plane, and h_q be the projection of the vector **A*B*** onto the image plane. The geometry of the set-up then implies a magnification

$$h_q = h_p(q/p) = s\sin(2\theta)(q/p), \qquad (1)$$

where p and q are the focal distances. Hence, the multilayer produces a magnified image of the diffracted intensity along the line defined by the incident beam. This image will be strongly tilted against the image plane and it might be more convenient to analyse the projection onto the image plane. Characterization of this projection may be performed by means of slit scans across the image plane.

The slope Ψ of the ideal elliptical shape of the focusing multilayer may be approximated by the Taylor expansion

$$\Psi(x_0 + \Delta x) = \Psi(x_0) + \frac{1}{R}\Delta x + \frac{3\theta_{\rm ML}(p^2 - q^2)}{8(pq)^2}\Delta x^2 + \frac{\theta_{\rm ML}(5p^3 - p^2q - pq^2 + 5q^3)}{16(pq)^3}\Delta x^3, \qquad (2)$$

with

$$1/R = \theta_{\rm ML}(p+q)/2pq. \qquad (3)$$

Here, $\theta_{\rm ML}$ and R are the glancing angle and radius of curvature, respectively, at position x_0. In general, the inclusion of second-order terms is sufficient.

The elliptic geometry implies that the glancing angle of the X-rays, $\theta_{\rm ML}$, will change along the multilayer. This must be compensated by an appropriate variation of the d-spacing (meridional grading). For reference we give the expansion up to the second order,

$$\frac{\Delta\theta}{\theta}(x_0 + \Delta x) = \frac{1}{2}\left(\frac{1}{q} - \frac{1}{p}\right)\Delta x + \frac{3p^2 - 2pq + 3q^2}{8(pq)^2}\Delta x^2. \qquad (4)$$

In practice, the focus will be broadened by various aberrations. Firstly, the perfection of the shape of the multilayer

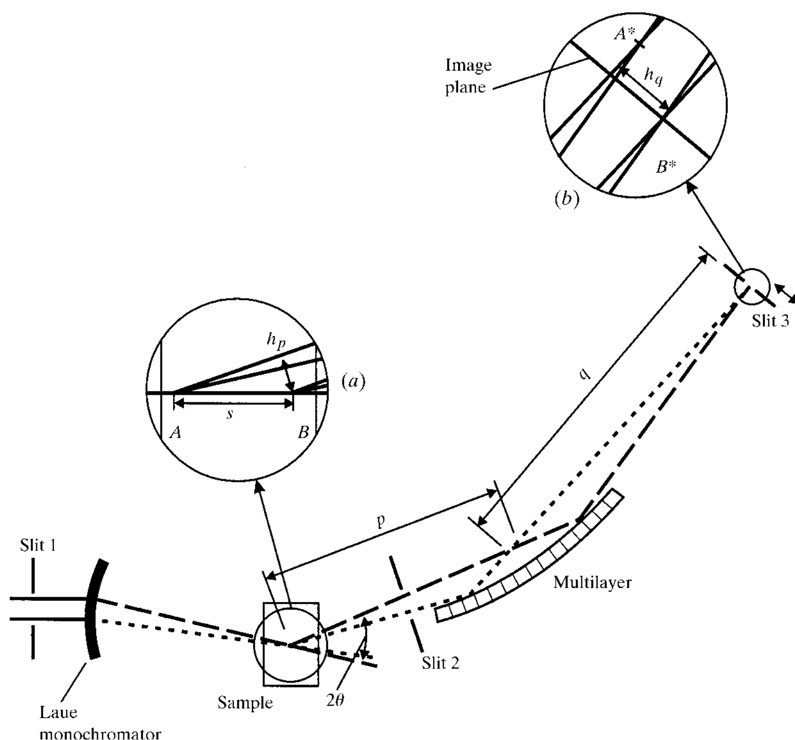

Figure 1
Sketch of the set-up used in the synchrotron test experiment. The energy band reflected by the focusing bent Laue crystal is indicated by long/short dashed lines which indicate low/high energy beams. The insets (a) and (b) clarify the focal properties in the object and image planes, respectively. Symbols are explained in the text.

is limited by the polishing errors. Slope errors of 1 μrad r.m.s. (root-mean-square) are typically achieved. Secondly, among the points in the sample only the one positioned at the actual focal point of the ellipse will be imaged ideally. Other points will be associated with some image broadening. Thirdly, the points A^*, B^* *etc.* in inset Fig. 1(*b*) lie in a plane, which is rotated with respect to the image plane. Unfortunately, the rotation angle is generally close to $\pi/2$, which makes slit scans in the A^*B^* plane impractical. Slit scans were therefore performed in the image plane, and the images consequently broadened by a factor proportional to h_q, *cf.* Fig. 1(*b*).

The optics principle presented here also applies for mirrors and aperiodic multilayers. Such components have the advantage that a longer line segment can be imaged, due to the increased bandwidth. However, the small critical angle for total external reflection complicates the use of mirrors at high energies.

3. Experimental set-up

The experiment was performed on the triple-axis diffractometer at the bending-magnet beamline BM5 at the ESRF synchrotron facility in Grenoble, France. The r.m.s. source size of this beamline is 126 μm and 37 μm in the horizontal and vertical planes, respectively.

The set-up with a horizontal scattering plane is illustrated in Fig. 1. A perfect Si(111) crystal was bent to a radius of curvature of 2.1 m and installed as a Laue monochromator on the first axis of the diffractometer. The crystal was asymmetrically cut to avoid a focal broadening by the crystal thickness (Schulze *et al.*, 1998). A set of crossed slits, slit 1, in front of the monochromator allowed for variation of the impinging beam dimensions. The vertical gap was set at 2 mm throughout, while the horizontal gap was varied between 0.3 mm and 1 mm during the experiment. The energy was set to 30.0 keV.

On the second axis a gold foil was mounted as a test sample. The foil had been cross-rolled to a high degree of deformation to obtain a powder sample with an almost random texture. It had a thickness of 21 μm, roughly corresponding to the penetration depth of the X-rays. It was placed in the focus of the monochromator with the surface perpendicular to the beam. The (222) powder line with a Bragg angle of $2\theta = 20.2°$ was used throughout.

On the third axis a bent (Ni, B_4C) multilayer was installed. It was 170 cm long, had a nominal d-spacing of 26.1 Å, and a meridional grading of $(\Delta d/d)/\Delta x = 0.38\ \mathrm{m}^{-1}$. It was mounted in a two-moment bender (Zhang *et al.*, 1998). By means of a long-trace profiler (Ziegler *et al.*, 1996) the shape of the central 100 mm had been optimized to an elliptic shape, as determined by the parameters p = 0.640 m, q = 1.254 m and a Bragg angle of θ_{ML} = 8.20 mrad. The corresponding radius of curvature is R = 103.4 m. The bending was associated with r.m.s. slope and shape errors of 1.5 μrad and 54 Å, respectively. Including parts of the surface closer to the clamps gave significantly poorer results, *e.g.* 3.2 μrad r.m.s. slope errors integrally over the central 150 mm. Hence, a crossed-slit system, slit 2, was installed in front of the multilayer to limit the illuminated length to 100 mm. The distance between the centre of the multilayer and slit 2 was 160 mm. The vertical gap of the slit was kept at 2 mm.

Distances were adjusted such that the sample was positioned in one of the focal points of the multilayer. In the other one, on an additional stage behind the diffractometer, a high-precision crossed-slit system, slit 3, was placed, with a scintillation detector behind it. By additional translations this unit could be moved in the horizontal plane, both along the beam and in a direction transverse to it. The precision

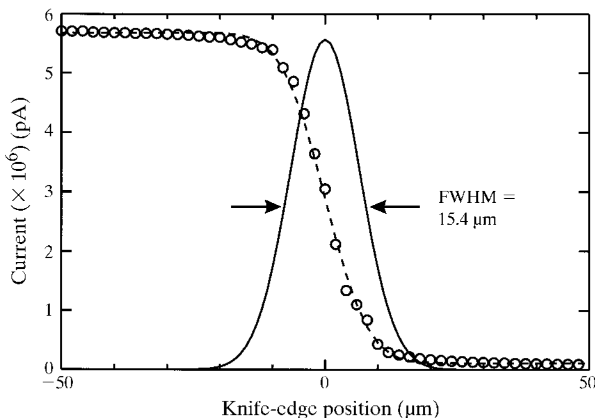

Figure 2
Monochromator focus: the result of a knife-edge scan through the focus of the bent Laue monochromator (circles), *cf.* Fig. 1. The intensity is measured by the current induced in an Si diode. The dashed line is a best fit of these data to an error function. The derivative of the fit is shown as a full line.

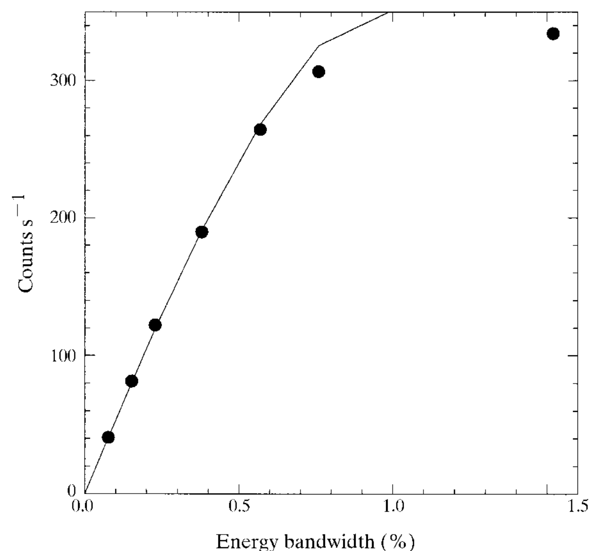

Figure 3
Reflectivity measurements: the detector count rate as a function of the energy bandwidth of the beam impinging on the Au test foil (circles). The full line shows a model calculation for an aberration-free multilayer with a Gaussian $\Delta d/d$ distribution with a width (FWHM) of 1.8%.

of the translations of the blades of slit 3 was found to be 1 µm or better. The vertical gap of slit 3 was kept fixed at 2 mm.

4. Experimental results

Initially the focal spot of the bent Laue monochromator was analysed. A W knife-edge was translated across the focus and the resulting intensity variation monitored by the current in an Si diode positioned behind the edge. The result for a horizontal gap of 0.5 mm of slit 1, corresponding to an energy band of 0.38%, is shown in Fig. 2. From a fit to an error function the FWHM (full width at half-maximum) was determined to be w = 15 µm. The width was independent of the horizontal gap of slit 1. For the case shown in Fig. 2 the flux in the focal spot was determined to be 10^{10} photons s^{-1} (100 mA)$^{-1}$. Next, q was optimized experimentally for p fixed at a distance of 1335 mm.

The reflectivity of the complete set-up, behind the multilayer, is illustrated in Fig. 3. Here the detector count rate is plotted as a function of the energy bandwidth of the incoming beam, as given by the horizontal gap of slit 1. (The count rate is normalized to a ring current of 100 mA.) For these measurements slit 3 was fully open horizontally. Also shown in Fig. 3 is the calculated response for an aberration-free multilayer with an assumed Gaussian-type bandwidth of $\Delta E/E$ = 1.8%. The response is scaled to the experiment, as no information on absolute reflectivity was obtained. The model describes the data well below a bandwidth of ~0.6%. Above this value the angular acceptance of slit 2 limits the signal.

The width of the central focal spot in the image plane was determined by a knife-edge scan within the image plane, using one of the blades in slit 3. The result, for a horizontal gap of 0.3 mm for slit 1, is shown in Fig. 4. Also shown is the expected response for aberration-free optics,

$$f(h_q) = \int_0^t \exp\left\{-\frac{4\ln 2}{w^2}\left[\frac{p}{q}\frac{h_q}{\cos(2\theta)} - x\tan(2\theta)\right]^2\right\} \mathrm{d}x. \quad (5)$$

Here t = 21 µm is the sample thickness, w = 15 µm is the width of the Gaussian-type Laue focus, and q/p is the magnification. Clearly the match is almost perfect.

Next, we estimated the depth resolution of the set-up. The horizontal gap of slit 3 was fixed at Δ = 8 µm and the effect of scanning the test foil along the monochromatic beam path was monitored. The result is shown in Fig. 5, along with the expected response for aberration-free optics. In this case the response may be expressed as

$$g(s) = \int_{-\Delta/2}^{\Delta/2} \mathrm{d}h_q \int_s^{s+t} \exp\left\{-\frac{4\ln 2}{w^2}\left[\frac{p}{q}\frac{h_q}{\cos(2\theta)} - x\tan(2\theta)\right]^2\right\} \mathrm{d}x, \quad (6)$$

where s is the translation of the sample along the monochromatic beam. Again a near-perfect match is observed. The FWHM width of the experimental curve is 44 µm. From (6), in the limit $t \to 0$, we infer that the depth resolution, FWHM, of the present set-up is 41 µm. From Fig. 5 we further infer that the depth resolution will be of the order of 10 µm or below, provided the gap of slit 3 and the monochromator spot both are infinitesimally narrow.

Finally, the imaging characteristics of the set-up were checked by translating the test foil in the direction of the monochromatic beam. For each position of the foil, knife-edge scans were made with slit 3 in a direction perpendicular to the diffracted beam. The resulting variations in focal shift are shown in Fig. 6 together with the expected response for an aberration-free system, $h_q = (q/p)\, s \sin(2\theta)$. The correspondence is good. The corresponding width of the images increased with distance to the focal point of the ellipse. The main contribution to this broadening was found to be related to the rotation of the plane containing points A^*, B^* *etc.* with respect to the image plane, *cf.* Fig. 1.

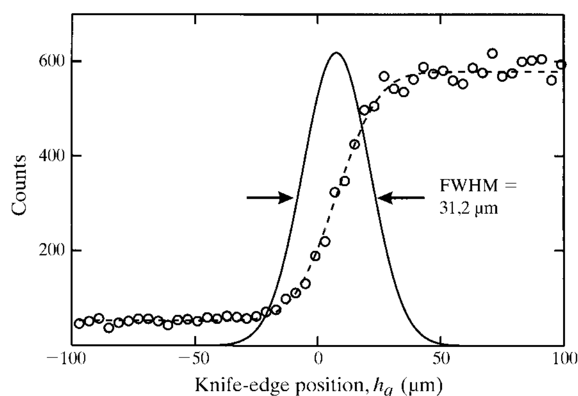

Figure 4
Image-plane focus: the result of a knife-edge scan through the focus of the image plane (circles), *cf.* Fig. 1. The dashed line represents the expected response for aberration-free optics, *cf.* equation (5). The derivative of the expected response is shown as a full line.

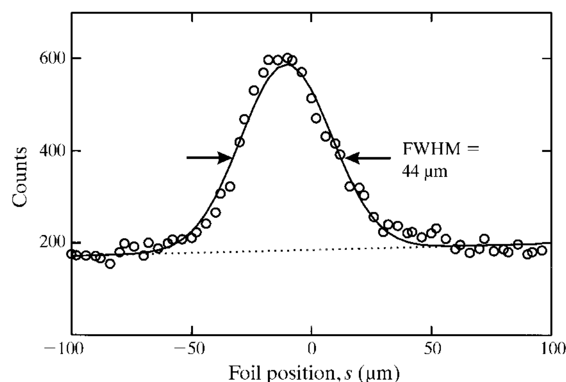

Figure 5
Depth resolution in the sample: the intensity through a centred slit in the image plane with an 8 µm gap upon translating the Au test foil in the direction of the monochromatic beam. Experimental data are plotted as circles. The full line represents the expected response for aberration-free optics, *cf.* equation (6). The dashed line is the best fit to a linear background.

5. Discussion

Throughout the analysis we have assumed that the slits and knife-edges are infinitely sharp. A full transmission study of each blade would be rather time consuming and has not been performed. Instead we estimate that the X-rays will partially penetrate the blades within a few micrometres from the edge. Hence, the focal spots are actually slightly narrower than indicated by the data points in Figs. 2, 4 and 5. With w slightly too large, the theoretical curves expressed by equations (5) and (6) will also be slightly too wide. These facts in turn imply that the depth resolution will be slightly better than inferred from Fig. 5. Moreover, the theory curve in Fig. 5 will tend to be more square-like, reminiscent of the shape of the sample, in accordance with the experimental data points. None of the conclusions of this work will be affected by these adjustments.

The experiment verified the optics principles as laid out in §2. However, the alignment of the set-up was tedious. If the technique is to be used in a standard way, new alignment algorithms based on, for example, the observed aberrations may be needed.

It should be emphasized that cost constraints made it necessary to use existing optics elements. In particular the multilayer substrate was rather thick. This prohibited a stronger bending and thereby the option of reducing slope error effects by shortening p. Also, the width of the focal spot of the Laue monochromator can be reduced considerably by changing the focal plane from the horizontal to the vertical.

The first use of the optics presented here may be in connection with the installation of a so-called three-dimensional X-ray microscope (3DXRD) at wiggler beamline ID11 at the ESRF (Kvick & Poulsen, 1997). Actually, this work is a pre-study within that context. The 3DXRD instrument will be dedicated to local materials science studies in thick specimens, and is to operate in the energy range 40–100 keV with a spatial resolution of $5 \times 5 \times 50\ \mu m^3$. To obtain three-dimensional information from such small volumes the incoming beam must be focused in both directions. At energies above 30 keV, this can be performed either by combining vertical focusing by a bent Laue crystal with horizontal focusing by means of a multilayer or alternatively by using two multilayers in a Kirkpatrick–Baez-type configuration (*e.g.* Underwood *et al.*, 1988). For comparison, at ID11 at 60 keV the flux in a $5 \times 5\ \mu m^2$ spot is estimated to be 8 and 500 times higher in these two cases than the flux reported here for the 30 keV $15 \times 2000\ \mu m^2$ line focus. The out-of-plane divergence introduced by such an extra focusing element will be smaller than the out-of-plane acceptance of the multilayer after the sample.

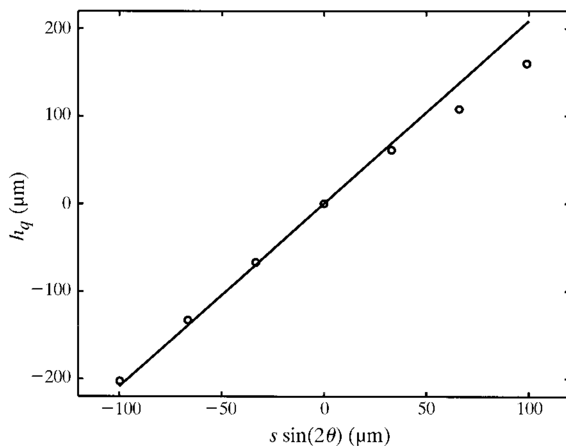

Figure 6
Shift of focal point, h_q, in the image plane upon translating the Au test foil a distance s in the direction of the monochromatic beam (circles). The straight line represents the expectation that the set-up will magnify the 2θ projection of s with a factor of q/p. The various symbols are defined in Fig. 1.

In the following we provide some comments on stress/strain characterization. A test of the new technique for such purposes was not performed due to space restrictions at the BM5 experimental station. Nevertheless we will comment on the prospect. The discussion will be restricted to the case where the local gauge volume contains a large number of randomly oriented grains. In practice, this assumption is often violated if the gauge volume is small. Oscillating the sample can then simulate a random orientation.

The conventional technique for stress and strain characterization is based on scanning a collimator, which is positioned after the sample. Alternatively, and more simple, a stationary slit is positioned closely behind the sample and the position of the diffracted beam is detected far behind the sample. These methods are associated with some systematic errors, as already mentioned in §1 (Webster *et al.*, 1996; Lorentzen, 1997). Firstly, common to both techniques, a shift in the centre of mass of the diffracting material within the local gauge volume will lead to a shift of the diffracted peak at the detector, and therefore an erroneous strain. Secondly, the slit may cut the high- or low-angle part of the diffracted beam, leading to asymmetric strain profiles with an erroneous centre of mass.

Instead we propose to use focusing optics after the sample and position a narrow slit at the focal point. The local strain is determined by the mean angular position of the X-rays that pass the slit. It can be measured by its position on a detector far behind the slit. The principle is analogous to the above-mentioned combination of a slit and a position-sensitive detector but the imaging properties of the multilayer allow placing the slit effectively infinitesimally close to the selected gauge volume. This method requires that the whole beam diffracted by the local gauge volume is accepted by the multilayer. In practice, the bandwidth and length of the multilayer can be made sufficiently large to meet this condition. For ideal aberration-free optics, either all or none of the X-rays from a particular point in the sample will pass through, and the systematic errors mentioned above will be avoided. In practice, as illustrated by the results presented here, aberrations are rather small close to the focal points and may be

controlled, *e.g.* by varying p. Hence, it seems that focusing optics may be a way to investigate local strain gradients across discontinuities. However, a conclusion on this item will have to await a test of strain measurements with the focusing analyser optics.

Finally, we emphasize that the focusing analyser principle presented will of course also apply for lower X-ray energies. In fact, it may be simpler to implement it in such cases, as Bragg angles will be larger and the multilayer may be substituted by a mirror. Towards higher energies, a limitation will arise by the decreasing Bragg angle and therefore acceptance of the multilayer. We expect that multilayers will be applicable up to about 100 keV.

6. Conclusions

An implementation of the focusing analysing principle by means of a bent and meridionally graded multilayer has been successfully tested. The concept of diffraction studies in millimetre-thick powder samples with a depth resolution of 10 µm seems within reach. Applications for investigations of surface-near areas (lower X-ray energies) can also be foreseen.

This work was sponsored by the Danish National Research Councils through the Engineering Science Center for ‘Structural Characterization and Modeling of Materials’ at Risø and through Dansync. The experiment was performed as part of the ESRF proposal MI-225. The authors would like to thank Palle Nielsen for his help in preparing the Au foils, and Ch. Morawe, R. Hustache and A. Rommeveaux for their help with bending, testing and mounting the multilayer. Fruitful discussions with D. Juul Jensen are acknowledged. In addition, we are very grateful for the general support by A. Freund to this project.

References

Allen, A. J., Hutchings, M. T., Windsor, C. G. & Andreani, C. (1985). *Adv. Phys.* **34**(4), 445–473.

Kvick, Å. & Poulsen, H. F. (1997). *Proceedings of the ESRF Workshop on Local Characterization of Materials by Synchrotron Radiation*, 13 February 1997. Grenoble: ESRF.

Lienert, U., Schulze, C., Honkimäki, V., Tschentscher, T., Garbe, S., Hignette, O., Horsewell, A., Lingham, M., Poulsen, H. F., Thomsen, N. B. & Ziegler, E. (1998). *J. Synchrotron Rad.* **5**, 226–231.

Lorentzen, T. (1997). *J. Neutron Res.* **5**, 167–180.

Poulsen, H. F., Garbe, S., Lorentzen, T., Juul Jensen, D., Poulsen, F. W., Andersen, N. H., Frello, T., Feidenhans'l, R. & Graafsma, H. (1997). *J. Synchrotron Rad.* **4**, 147–155.

Schulze, C., Lienert, U., Hanfland, M., Lorenzen, M. & Zontone, F. (1998). *J. Synchrotron Rad.* **5**, 77–81.

Underwood, J. H., Thomson, A. C., Wu, Y. & Giauque, R. D. (1988). *Nucl. Instrum. Methods Phys. Res. A*, **266**, 269–302.

Webster, P. J., Mills, G., Wang, X. D., Kang, W. P. & Holden, T. M. (1996). *J. Neutron Res.* **3**, 223–240.

Zhang, L., Hustache, R., Hignette, O., Ziegler, E. & Freund, A. (1998). *J. Synchrotron Rad.* **5**, 804–807.

Ziegler, E., Hignette, O., Lingham, M. & Souvorov, A. (1996). *Proc. SPIE*, **2856**, 61–67.